Spark-plasma-sintering of double-walled carbon nanotube–magnesia nanocomposites

Felipe Legorreta Garcia, Claude Estournès, Alain Peigney, Alicia Weibel, Emmanuel Flahaut, Christophe Laurent

Spark-plasma-sintering of double-walled carbon nanotube–magnesia nanocomposites

F. Legorreta Garcia, C. Estournès, A. Peigney, A. Weibel, E. Flahaut and Ch. Laurent*

Université de Toulouse, CIRIMAT, UMR CNRS-UPS-INP, Bât. 2R1, Université Paul-Sabatier, 31062 Toulouse Cedex 9, France

A double-walled carbon nanotube–MgO powder is prepared without any mixing. The applied pressure is the main parameter acting on densification. Increasing the maximum temperature and holding time is marginally beneficial. The nanotubes are blocking the matrix grain growth. The nanocomposite prepared using the most severe spark plasma sintering conditions (1700 °C, 150 MPa) shows mostly undamaged nanotubes and a higher microhardness than the other materials, reflecting a better bonding between nanotubes and matrix. The electrical conductivity of all nanocomposites is over 12 S/cm.

Keywords: Spark plasma sintering; Carbon nanotubes; Nanocomposite; Magnesia

Amongst the many possible applications of carbon nanotubes (CNTs) are ceramic–matrix nanocomposites [1]. The first difficulty for a successful preparation is to obtain a homogeneous distribution of undamaged CNTs into the composite powder. To overcome the need for a mechanical-mixing step during the powder preparation, a direct method for the *in situ* synthesis of the CNTs into an Al_2O_3 matrix has been proposed [2]. It is based on a catalytic chemical vapor deposition (CCVD) route involving the reduction in H_2–CH_4 of Al_2O_3–Fe_2O_3 solid solutions, producing CNT–Fe–Al_2O_3 nanocomposite powders. The reduction first produces Fe nanoparticles that are active for the decomposition of CH_4, and subsequently for the formation of CNTs if their diameter is small enough ($\leqslant$5 nm) [3,4]. This method was expanded to $MgAl_2O_4$ and MgO matrix [5,6] composite powders.

The second difficulty is to densify the composite powder without damaging the CNTs. The most common method is hot-pressing (HP). Most works [7,8,9,10,11,12,13,14] report that increasing contents of CNTs inhibit the densification of the material, when compared to the corresponding oxide. It has been shown [9] that a low CNTs content favors the grain rearrangement (first shrinkage step), probably owing to a lubricating role which facilitates the sliding at grain contacts or grain boundaries. By contrast, for higher contents, CNTs form a rigid web structure, therefore inhibiting the rearrangement process. In the second sintering step, CNTs inhibit the shrinkage, leading to decreasing densifications.

* Corresponding author; e-mail: laurent@chimie.ups-tlse.fr

The spark plasma sintering (SPS) technique has been reported as an efficient method to achieve the total densification of CNT-oxide composites without damaging the CNTs [15,16,17,18,19,20,21]. Full densification can be reached with SPS at comparatively lower temperature with substantial shorter holding time. However, this supposes that matrix grains are nonagglomerated and a few tens of nanometers in size.

This paper is focused on CNT–MgO composites. Micrometric MgO powders require elevated temperatures above 1500 °C for full densification by natural sintering or HP [22] and show a dramatic increase in grain size [23]. Decreasing the particle size allows a dramatic decrease in the HP sintering temperature and grain growth [24,25,26]. The same group [27,28] also reported that a 11-nm powder was fully densified by SPS at 800 °C (150 MPa), with only moderate grain growth (52 nm).

The first attempts of the present authors at the densification of CNT–MgO composites by HP [8,29] revealed that it is necessary to use a temperature of 1600 °C in order to increase the densification, which reached 93%, but this destroys most CNTs. Thus, the present paper aims at investigating for the first time the SPS densification of a CNT–MgO powder. Compared to our early works [8,29], the powder quality was much improved: the CNTs are essentially DWNTs and the MgO grain size is below 100 nm. The microstructure of the DWNT–MgO composites is investigated. The electrical conductivity and the Vickers microhardness are also reported.

The synthesis of the DWNT–MgO nanocomposite powder was reported elsewhere [6]. The powder of cata-

doi:10.1016/j.scriptamat.2008.12.053

lytic material $Mg_{0.99}(Co_{0.75}Mo_{0.25})_{0.01}O$ was prepared by the combustion route using citric acid as the fuel and the appropriate amounts of $Mg(NO_3)_2{\cdot}6H_2O$, $Co(NO_3)_3{\cdot}9H_2O$ and $(NH_4)_6Mo_7O_{24}{\cdot}4H_2O$. For the sake of comparison, a powder of MgO was prepared by the same method. The catalytic material was submitted to a CCVD treatment (H_2–CH_4 with 18 mol.% CH_4, maximum temperature 1000 °C, heating and cooling rates 5 °C/min, no dwell) producing the DWNT–MgO nanocomposite powder. The carbon content (7.0 ± 0.2 wt% corresponding to 14 vol.%) was determined by flash combustion. Field-emission-gun scanning electron microscopy (FEG-SEM, JEOL JSM 6700F) images of the DWNT–MgO composite powder show that the MgO matrix is made up of micrometric platelet-like agglomerates (Fig. 1a), made up of primary grains ⩽100 nm (Fig. 1b). Transmission electron microscopy (TEM, Jeol JEM 1011) observation showed CNTs bundles (Fig. 1c) up to 50 nm in diameter, in fairly high quantity. An earlier study [6] revealed that about 80% of the CNTs are DWNTs (with 15% single- and 5% triple-walled CNTs), with outer diameters in the range 1–3 nm and inner diameters in the range 0.5–2.5 nm.

The high-frequency range (1100–1800 cm^{-1}) of the Raman spectrum (Jobin-Yvon LabRAM HR 800, 632 nm, five Raman spectra-averaged for each sample) (Fig. 1d) shows the D band (*ca.* 1320 cm^{-1}) and a complex G band (*ca.* 1589 cm^{-1}). The ratio between the intensity of the D and the G bands, $I_{D/G}$, is equal to 0.18. An increasing $I_{D/G}$ value corresponds to a higher proportion of sp^3-like carbon, which is generally attributed to the presence of more structural defects. The radial breathing modes (RBM) are observed in the low-frequency range (100–300 cm^{-1}) of the spectrum (inset in Fig. 1d). The peak frequencies are inversely proportional to the CNTs diameters. The detected diameters are in the range 0.9–2.2 nm.

Consolidation was performed by SPS (Dr Sinter 2080, SPS Syntex Inc., Japan). Samples of the CNT-MgO powder were loaded into a 15-mm inner diameter graphite die. A sheet of graphitic paper was placed between the punch and the powder as well as between the die and the powder for easy removal. The powders were sintered in a vacuum (residual cell pressure <5 Pa). A pulse configuration of 12 pulses (one pulse duration 3.3 ms) followed by two periods (6.6 ms) of zero current was used. Heating rates of 150 °C/min and 100 °C/min were used from room temperature to 600 °C and from 600 to the maximum temperature (1550–1700 °C), respectively, where a dwell (0–30 min) was applied. An optical pyrometer, focused on a little hole at the surface of the die, was used to measure the temperature.

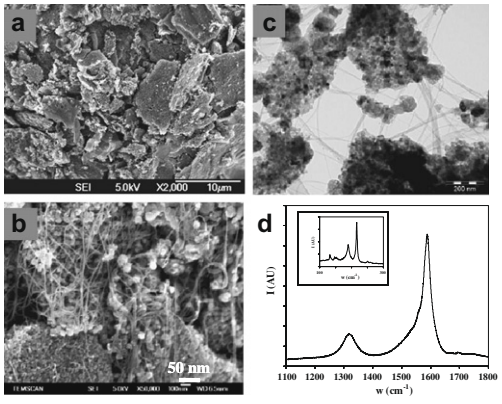

Figure 1. FEG-SEM images (a and b) and a TEM image (c) of the DWNT–MgO powder and (d) the high-frequency range of the Raman spectrum with (inset) the low-frequency range.

A uniaxial pressure (100–150 MPa) was applied from 1000 °C upwards and maintained during the dwell. Natural cooling was applied. The uniaxial pressure was gradually released during cooling. The maximum SPS temperature was first fixed at 1550 °C and the influence of SPS pressure and dwell time were investigated. Six samples (A–F in Table 1) were prepared. The sintered pellets (15 mm diameter, 3 mm thick) were polished with a diamond paste up to 0.5 μm. The density was evaluated by the Archimedes method. The densifications (d ± 0.6%) were calculated using a full density equal to 3.55 (taking 1.8 for DWNTs and supposing that Co- and Mo-species, which account for very small quantities, are present as metallic Co and Mo_2C, respectively). The densification is in the range 85.9–90.2% and it increases with the applied pressure (Table 1), probably because this favors the crushing of matrix agglomerates and also contributes to help the grain rearrangement which is inhibited by the CNTs network. Increasing the dwell time moderatly favors the densification, the more so for a lower pressure (A and B) than for a higher pressure (E and F).

The XRD patterns (Cu K_α radiation, Bruker AXS-D4 Endeavor, not shown) reveal the MgO peaks, two weak peaks corresponding to Mo_2C and a very weak, wide peak corresponding the (002) graphite planes accounting for the DWNTs. Raman spectra (not shown) were recorded for E and F (polished surfaces). The G band is more narrow than for the powder but the peak is not shifted to a higher wavenumber, which could indicate the absence of residual stresses that may be imposed by the matrix [16]. $I_{D/G}$ is about twice that for the starting powder, which could indicate some degree of damage to the DWNTs. However, RBM are still observed.

FEG-SEM images of the fracture surface (Fig. 2a–c) and the polished surface (Fig. 2d) reveal no significant difference in microstructure between the different compos-

Table 1. SPS parameters (maximum temperature *T*; time at maximum temperature *t*, pressure *P*), densification (*d*), electrical conductivity (σ), average Vickers microhardness (HV) and minimum and maximum HV (HV_{min}/HV_{max}, respectively) for the DWNT–MgO nanocomposites and MgO.

Specimen	*T* (°C)	*t* (min)	*P* (MPa)	*d* ± 0.6 (%)	σ (S cm^{-1})	HV	HV_{min}/HV_{max}
A	1550	0	100	85.9	–	–	–
B	1550	3	100	87.1	–	–	–
C	1550	5	130	88.3	–	–	–
D	1550	1	138	88.1	–	–	–
E	1550	5	150	89.5	13	551	425/675
F	1550	30	150	90.2	15	549	351/818
G	1600	5	150	91.0	13	507	381/585
H	1600	30	150	91.0	12	571	383/699
I	1650	5	150	90.2	12	615	366/853
J	1650	30	150	90.3	17	582	471/895
K	1700	5	150	90.4	14	776	497/988
L	1700	30	150	91.2	15	972	773/1148
MgO	1650	5	150	98.3	–	746	689/808

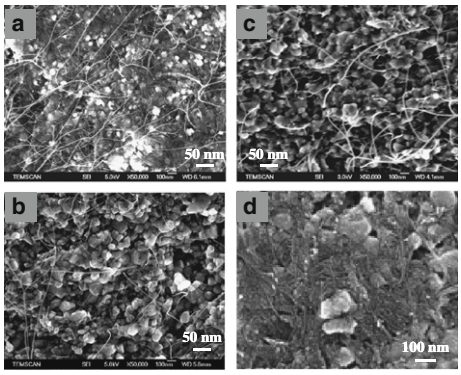

Figure 2. FEG-SEM images of the fracture surface for the DWNT–MgO nanocomposites prepared by SPS at 1550 °C. (a) A; (b) E; (c) F and (d) the polished surface of D.

ites. The DWNTs and DWNTs bundles are well dispersed and are observed in all examined areas. They do not appear to be damaged. The MgO matrix grains are not larger than 100 nm, i.e. a size similar to that in the powder, indicating that no significant grain growth occured at 1550 °C, whatever the dwell time and pressure.

In a second part of the study, the influence of the maximum temperature was investigated, using a pressure equal to 150 MPa. Six more composites (G-L) were prepared in addition to the already-studied E and F specimens (Table 1). For the sake of comparison, the MgO powder was sintered in he same conditions than specimen I.

The densification for MgO (98.3%) is significantly higher than for the A-F composites. However, the densifications for the composites (89.5–91.2%, - Table 1), are only marginaly higher and there is no obvious effect of either temperature or time. Raman spectra were recorded for the G-L composites (polished surfaces) and the results are essentially similar to those reported above for E and F. The spectrum for L, prepared using the most severe SPS conditions is shown in Fig. 3. $I_{D/G}$ is equal to 0.34. No particular trend was found for a $I_{D/G}$ increase with either increasing temperature or time. RBM are still observed in the low-frequency range of the spectra (inset in Fig. 3).

FEG-SEM observation of the fracture surface for MgO (Fig. 4a) reveals that the grain size is *ca.* 31 μm. Thus, densification was possible because there was a strong grain growth. By contrast, FEG-SEM images of the fracture surface for the composites (Fig. 4b–d) show results that are similar to those found for A-F. Firstly, the MgO matrix grains are still $\leqslant$ 100 nm. This confirms that a high proportion of CNTs totally hinders the matrix grain growth, particularly when they are well distrib-

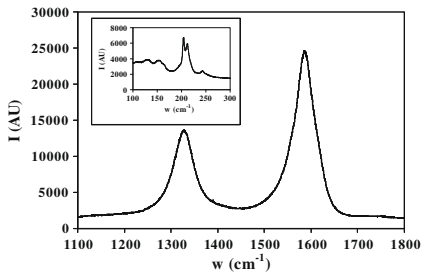

Figure 3. High-frequency range of the Raman spectrum of the polished surface of composite L and (inset) the low-frequency range.

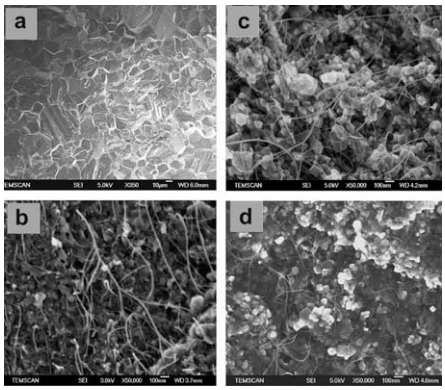

Figure 4. FEG-SEM images of the fracture surface for (a) MgO; (b) composite G; (c) composite I; (d) composite K. Bar = 10 μm for (a) and 100 nm for (b–d).

uted between the matrix grains. Secondly, the DWNTs appear mostly undamaged, even using a SPS temperature equal to 1700°C. This is in sharp contrast with earlier results using HP [8,29], where the CNTs were strongly damaged at 1600 °C. This may be due to the better quality of the present DWNTs and to the shorter time when using SPS.

The electrical conductivity was measured at room temperature with d.c. currents on ($1.6 \times 1.6 \times 8\ mm^3$) specimens parallel to their length, i.e. perpendicular to the pressing axis. The current densities used were lower than 160 mA/cm^2 (Keithley 2400). The electrical conductivity (σ-Table 1) for the E-L composites is in the range 12–17 S/cm, with no significant difference between the materials. These values are in line with other results [8,20,30,31,32,33]. CNTs confer an electrical conductivity to a composite with an insulating matrix [8] and the electrical percolation threshold is fairly low (< 1 vol.%) owing to their very high aspect ratio (> 10,000) of the CNTs [33]. This result confirms the above electron microscopy observations showing that the DWNTs are not damaged even when using the most severe SPS conditions.

The indentation tests (5 N for 10 s in air at room temperature) were performed on the polished surface of the specimens by loading with a Vickers indenter (Shimadzu HMV 2000). The calculated values are the average of 10 measurements. The Vickers microhardness (HV - Table 1) for MgO is equal to 746 whereas it is in the range 549–615 for composites E-J, which could reflect their lower densification.

By contrast, a similar value (HV = 776) is found for specimen K and a significantly higher value (HV = 972) is found for specimen L, despite a densification significantly lower for both materials than for MgO. Interestingly, the minimum and maximum values are also higher for L (Table 1) than for the other materials. Note that all composites contain the same amount of Co and Mo_2C. Because of the relative proportions of the metals in the starting material, the influence of Co and Mo_2C is negligible. The influence of CNTs on the microhardness of CNT-oxide composites is not clearly established in the literature but the method by which the composite powder is prepared appears to be very important. Processing-induced changes in the matrix may have greater effects on mechanical properties than the actual presence

of CNTs [34]. Indeed, when starting from powders prepared by mechanical mixing of powders or powder suspensions, it was reported [15,16,19,31] that the microhardness decreases with increasing proportions of CNT bundles, which was related to the simultaneous decrease in densification. In addition, it was shown [16] that CNT-Al_2O_3 composites are highly resistant to damage contact, also explaining the microhardness decrease.

By contrast, An et al. [10] have used a method where CNTs are formed *in situ* in the Al_2O_3 matrix, i.e. a route roughly similar to the present one, and have reported for HP composites a regular increase in microhardness when the CNTs content was increased up to 4 wt.%. This was related to a lower matrix grain size, but without ruling out a possible CNTs reinforcement effect. Other researchers [18] have used methods where the matrix is synthesized *in situ* around the CNTs and have also reported that the microhardness increases up to a certain CNTs fraction but that CNTs agglomeration for higher loadings causes a decrease. These researchers [18] proposed that owing to their particular powder preparation route, as opposed to mechanical mixing, the CNTs were well-dispersed within, and strongly bonded with the alumina grains, which made possible an effective load transfer from the matrix grains to the CNTs. Thus, it is possible that in the present case, the higher microhardness observed for specimen L is due to a combination of the use of the higher SPS temperature (1700 °C) and longer time (30 min), which would favor a better bonding between the DWNTs and the MgO grains. Indeed, the E-J composites sintered at a lower temperature do not show the microhardness increase although they have the same DWNTs content, MgO grain size and densification than composite L.

In conclusion, DWNT-MgO nanocomposite powders prepared by an *in situ* synthesis route (14 vol.% DWNTs) are consolidated by SPS without damaging the DWNTs, by contrast to earlier results using HP. The very high homogeneity of the dispersion of the DWNTs may result in an increased difficulty to reach higher densifications (maximum about 90%). An increased pressure (up to 150 MPa) probably enhances the crushing of the MgO matrix agglomerates made up of crystallites $\leqslant$ 100 nm and also contributes to help the rearrangement inhibited by the DWNTs network. However, the increase in both the maximum temperature (up to 1700 °C) and holding time (up to 30 min) is only marginally beneficial because the network of DWNTs totally blocks the matrix grain growth. By contrast, for pure MgO (150 MPa, 1650 °C), the densification is equal to 98.3% and the grain size is about 31 μm. The electrical conductivity of the nanocomposites is in the range 12–17 S/cm owing to the percolation of the DWNTs. A much higher Vickers microhardness (HV = 972) is observed for the specimen sintered in the most severe SPS conditions, despite it has the same DWNTs content, MgO grain size and densification than the other nanocomposites. This could reflect a better bonding between the DWNTs and the MgO grains. Further studies will address the problem using powders containing a lower amount of DWNTs and also investigate the toughness of such materials.

The authors thank L. Datas and L. Weingarten for assistance with the electron microscopy performed at TEMSCAN, the "Service Commun de Microscopie Electronique à Transmission", Université Paul-Sabatier. The SPS was performed at the Plateforme Nationale CNRS de Frittage-Flash (PNF^2, Toulouse).

[1] A. Peigney, Ch. Laurent, in: I.M. Low (Ed.), Ceramic Matrix Composites: Microstructure Properties Applications, Woodhead Publishing Ltd, Cambridge, 2006, p. 309.
[2] A. Peigney, Ch. Laurent, F. Dobigeon, A. Rousset, J. Mater. Res. 12 (1997) 613.
[3] J.H. Hafner, M.J. Bronikowski, B.K. Azamian, P. Nikolaev, A.G. Rinzler, D.T. Colbert, K.A. Smith, R.E. Smalley, Chem. Phys. Lett. 296 (1998) 195.
[4] A. Peigney, P. Coquay, E. Flahaut, R.E. Vandenberghe, E. De Grave, Ch. Laurent, J. Phys. Chem. B 105 (2001) 9699.
[5] E. Flahaut, A. Peigney, Ch. Laurent, A. Rousset, J. Mater. Chem. 10 (2000) 249.
[6] E. Flahaut, R. Bacsa, A. Peigney, Ch. Laurent, Chem. Commun. (2003) 1442.
[7] Ch. Laurent, A. Peigney, O. Dumortier, A. Rousset, J. Eur. Ceram. Soc. 18 (1998) 2005.
[8] E. Flahaut, A. Peigney, Ch. Laurent, Ch. Marlière, F. Chastel, A. Rousset, Acta Mater. 48 (2000) 3803.
[9] A. Peigney, S. Rul, F. Lefèvre-Schlick, Ch. Laurent, J. Eur. Ceram. Soc. 27 (2007) 2193.
[10] J.W. An, D.H. You, D.S. Lim, Wear 255 (2003) 677.
[11] J. Ning, J. Zhang, Y. Pan, J. Guo, Mater. Sci. Eng. A 357 (2003) 392.
[12] A.R. Boccaccini, D.R. Acevedo, G. Brusatin, P. Colombo, J. Eur. Ceram. Soc. 25 (2005) 1515.
[13] Q. Huang, L. Gao, J. Mater. Chem. 14 (2004) 2536.
[14] J. Fan, D. Zhao, M. Wu, Z. Xu, J. Song, J. Am. Ceram. Soc. 89 (2006) 750.
[15] G.-D. Zhan, J.D. Kuntz, J. Wan, A.K. Mukherjee, Nature Mater. 2 (2003) 38.
[16] X. Wang, N.P. Padture, H. Tanaka, Nature Mater. 3 (2004) 539.
[17] J. Sun, L. Gao, W. Li, Chem. Mater. 14 (2002) 5169.
[18] S.I. Cha, K.T. Kim, K.H. Lee, C.B. Mo, S.H. Hong, Scripta Mater. 53 (2005) 793.
[19] J. Sun, L. Gao, M. Iwasa, T. Nakayama, K. Niihara, Ceram. Int. 31 (2005) 1131.
[20] S.-L. Shi, J. Liang, J. Appl. Phys. 101 (2007) 023708.
[21] Q. Huang, L. Gao, Y. Liu, J. Sun, J. Mater. Chem. 15 (2005) 1995.
[22] J.M. Vieira, R.J. Brook, J. Am. Ceram. Soc. 67 (1984) 450.
[23] C. Aksel, B. Rand, F.L. Riley, P.D. Warren, J. Eur. Ceram. Soc. 22 (2002) 745.
[24] Y. Feng, D. Agrawal, G. Skandanand, M. Jain, Mater. Lett. 58 (2004) 551.
[25] A. Itoh, K. Itatani, F.S. Howell, A. Kishioka, M. Kinoshita, J. Mater. Sci. 31 (1996) 2757.
[26] D. Ehre, E.Y. Gutmanas, R. Chaim, J. Eur. Ceram. Soc. 25 (2005) 3579.
[27] R. Chaim, Z. Shen, M. Nygren, J. Mater. Res. 19 (2004) 2527.
[28] R. Chaim, M. Margulis, Mater. Sci. Eng. A 407 (2004) 180.
[29] A. Peigney, E. Flahaut, Ch. Laurent, F. Chastel, A. Rousset, Chem. Phys. Lett. 352 (2002) 20.
[30] G.-D. Zhan, J.D. Kuntz, J.E. Garay, A.K. Mukherjee, Appl. Phys. Lett. 83 (2003) 1228.
[31] G.-D. Zhan, A.K. Mukherjee, Int. J. Appl. Ceram. Technol. 1 (2004) 161.
[32] L. Jiang, L. Gao, Chem. Mater. 15 (2003) 2848.
[33] S. Rul, F. Lefèvre-Schlick, E. Capria, Ch. Laurent, A. Peigney, Acta Mater. 52 (2004) 1061.
[34] W.A. Curtin, B.W. Sheldon, Mater. Today 7 (2004) 44.